Int. J. Mech. Sci. Vol. 31, No. 4, pp. 285–300, 1989
Printed in Great Britain.

0020-7403/89 $3.00 + .00

INVESTIGATION OF SHEET METAL FORMING BY BENDING—PART I. AXISYMMETRIC ELASTIC–PLASTIC BENDING OF CIRCULAR SHEETS PRESSED BY CYLINDRICAL PUNCHES

L. C. ZHANG,* T. X. YU† and R. WANG†

*Department of Mechanics, Zhejiang University, Hangzhou, China and †Department of Mechanics, Peking University, Beijing, China

(*Received* 24 *June* 1988; *and in revised form* 1 *October* 1988)

Abstract—This paper thoroughly investigates the axisymmetric deformation mechanism of workpieces in conical cup tests using the modified adaptive Dynamic Relaxation method (maDR method), and finds many important mechanical features of them. In addition, it proposes a simple approximate analytical model for engineers.

NOTATION FOR PARTS I TO IV

b initial radius of a workpiece
$\mathbf{C}$ damping matrix
c proportionality coefficient between $\mathbf{C}$ and $\mathbf{M}$
E Young's modulus
E_s^0 secant modulus
E_t^0 tangent modulus
e_{ij} deviatoric strain component
$\mathbf{F}$ generalized force vector
G shear modulus
h thickness of sheet
h^* work-hardening modulus
J_2 the second invariant of the deviatoric stress tensor
K_r, K_θ curvatures in the r- and θ-directions
$\mathbf{M}$ mass matrix
M_b bending moment at the periphery
M_r, M_θ bending moments in the r- and θ-directions
N_b reacting force at the periphery
N_r, N_θ membrane forces in the r- and θ-directions
$\mathbf{P}$ rigidity matrix
q external load
$\mathbf{R}$ residual vector in equations (3) and (4) of Part I
S_{ij} deviatoric stress component
$\mathbf{T}$ a vector composed by stresses, defined by equation (11) of Part III
u radial mid-plane displacement
u_b radial mid-plane displacement at the periphery
w deflection
$\mathbf{X}$ generalized displacement vector
Y initial yield stress
Z direction normal to the mid-plane of sheet
ε strain
ζ boundary between the elastic and plastic regions
θ semi-angle of a conical die; coordinate in the circumferential direction
μ friction coefficient
ν Poisson's ratio
σ stress
ϕ Mises loading function

superscripts

^{0} mid-plane
$^-$ loading coordinate system (LCS), see Part III
$^\sim$ at the end of loading process in LCS, see Part III
* unloading coordinate system (UCS), see Part III

subscripts

r r-direction
z z-direction
θ θ-direction

1. INTRODUCTION

It is important for production engineers carrying out sheet metal forming processes to select sheet materials appropriately and to design forming tools successfully, assuring both the required final shapes and the claimed service properties of their workpieces. However, it is not easy to do so, because many factors—such as material behaviour of the sheet metal, forming conditions, formability criterion adopted, etc.—need to be considered. Moreover, such factors often affect each other, so that one needs to have a comprehensive view for controlling an optimal process from design to operation. Obviously, it presupposes an exact understanding of the action of each factor: for instance, the effects of punch and die geometries, springback, wrinkling, lubrication and so on.

However, there exist many difficulties in investigating these problems, owing to their complicated characters in coupling non-linearities of geometry and material behaviour. In recent years, although there have been many advances in the applications of numerical techniques to analysing the forming processes, very large computation time is required. It should also be noted that many problems cannot be solved by numerical methods and large computers only, but depend on establishing correct mechanical concepts and appropriate analytical models. The prediction of the plastic wrinkling of a sheet during forming operation is a good example; it is related to the well-known plastic buckling paradox of plates and shells—i.e. why it is usually the case that better theoretical predictions of plastic buckling load are given by the deformation theory rather than the incremental theory of plasticity.

In this series of four papers, the authors will discuss these problems. In the present paper, the authors investigate thoroughly the whole axisymmetric deformation of the workpieces in conical die cup tests, which are a kind of standard test in production engineering for evaluating the formability of sheet metals. It reveals how plastic regions in a workpiece appear and spread, and how they vary with punch diameter. The paper also shows the distributions of strains and internal forces, and proposes a simple approximate model for engineers that can analyse the deformation of such workpieces and evaluate the formability of metal materials. All of the present numerical analyses are carried out by the maDR method [1], which was recently developed by the authors and has good prospects for engineering applications.

2. THE maDR METHOD

Unlike other methods, the maDR method is based on the fact that the static solution of a mechanical system is the steady-state part of the transient response to step loading. Accordingly, the governing equation describing a static mechanics problem

$$\mathbf{P}(\mathbf{X}) = \mathbf{F} \tag{1}$$

is changed into a corresponding one for dynamics:

$$\mathbf{M}\ddot{\mathbf{X}} + \mathbf{C}\dot{\mathbf{X}} + \mathbf{P}(\mathbf{X}) = \mathbf{F}. \tag{2}$$

The mass matrix $\mathbf{M}$ and the damping matrix $\mathbf{C}$, because we are not interested in the dynamic process of the system, are fictitiously chosen so that the static solution is obtained in a minimum number of pseudo-time increment steps. Therefore, one often chooses $\mathbf{M}$ and $\mathbf{C}$ as diagonal matrices and makes $\mathbf{C} = c\mathbf{M}$. In so doing, one obtains explicit iteration formulae for finding the solution vector $\mathbf{X}$ when the central difference scheme with respect to pseudo-time t is used:

$$\dot{\mathbf{X}}^{n+1/2} = \frac{2-\tau^n c^n}{2+\tau^n c^n}\dot{\mathbf{X}}^{n-1/2} + \frac{2\tau^n}{2+\tau^n c^n}\mathbf{M}^{-1}\mathbf{R}^n, \tag{3a}$$

and $$\mathbf{X}^{n+1} = \mathbf{X}^n + \tau^{n+1}\dot{\mathbf{X}}^{n+1/2}, \tag{3b}$$

where τ^n is the pseudo-time increment of the nth iteration,

$$\mathbf{R}^n = \mathbf{F} - \mathbf{P}(\mathbf{X}^n), \tag{4a}$$

$$\dot{\mathbf{X}}^{n-1/2} = (\mathbf{X}^n - \mathbf{X}^{n-1})/\tau^n, \tag{4b}$$

and

$$\ddot{\mathbf{X}}^n = (\dot{\mathbf{X}}^{n+1/2} - \dot{\mathbf{X}}^{n-1/2})/\tau^n. \tag{4c}$$

The differences between the DR (refer to [2], for instance) and maDR methods are in the calculation of c^n and $\mathbf{X}^0$. In the latter, c^n is calculated as

$$c^n = 2\left\{\frac{(\mathbf{X}^n)^t\mathbf{P}(\mathbf{X}^n)}{(\mathbf{X}^n)^t\mathbf{M}\mathbf{X}^n}\right\}^{1/2}, \tag{5}$$

and the each element x_i^0 of the initial vector $\mathbf{X}^0$ is obtained in such a way that $x_i^0 = (x_i^* + x_i^{**})/2$, where x_i^* and x_i^{**} are the values of two neighbouring but opposite peaks of the locus of x_i determined by putting $c = 0$. These treatments make the maDR method more efficient than the DR method. Furthermore, to guarantee numerical stability, the elements of M are determined by the Gerschgörin theorem. Compared with other methods, maDR has the following conspicuous features:

(i) there is no need to treat large scale equations; instead, one can obtain solutions with simple explicit iterations; this makes it possible to solve complicated problems with a small computer;
(ii) it is very reliable for seeking an equilibrium state.

3. DEFORMATION ANALYSIS OF WORKPIECES IN CONICAL CUP TESTS

A workpiece in a conical cup test, see Fig. 1(a), can be idealized by the model shown in Fig. 1(b). The action of the cylindrical punch is considered as a ring load p acting at a radius equal to that of the punch, r_p. If it is assumed that the friction between the workpiece and the conical die is determined by the formula

$$\text{friction force} = (\text{friction coefficient } \mu)\cdot(\text{normal force on die cone}), \tag{6}$$

where μ was measured experimentally with no lubrication applied, the boundary forces can be expressed as

$$N_b = -\frac{pr_p(\cos\theta - \mu\sin\theta)}{(b + u_b)(\sin\theta + \mu\cos\theta)} \tag{7a}$$

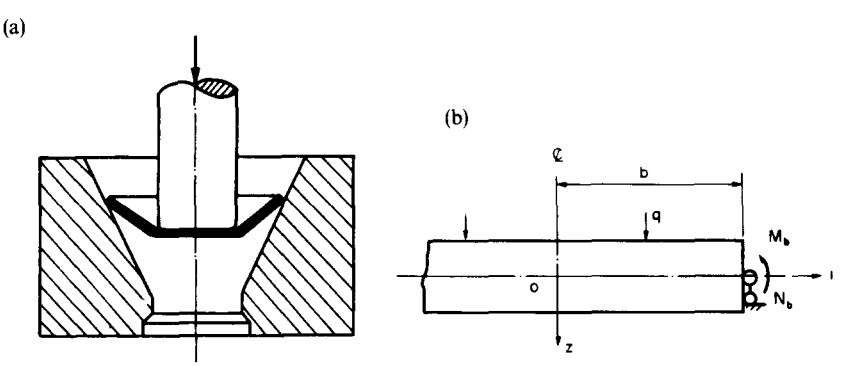

FIG. 1. (a) Schematic diagram of the conical cup test. (b) Mechanical model of the workpiece.

and

$$M_b = \tfrac{1}{2} h N_b, \tag{7b}$$

where θ is the semi-angle of the conical die, h and b are the thickness and initial radius of the workpiece, respectively, and u_b is the radial mid-plane displacement at the periphery. Cylindrical coordinates are adopted, and the well-known Kirchhoff assumption for thin plates is taken throughout the present analysis.

3.1. *Basic equations*

3.1.1. *Equilibrium equations.* The equilibrium equations including membrane forces in incremental form during an axisymmetric deformation process can be written as

$$\begin{cases} \dfrac{\partial \delta N_r}{\partial r} + \dfrac{1}{r}(\delta N_r - \delta N_\theta) = 0, \\ \dfrac{\partial^2 \delta M_r}{\partial r^2} + \dfrac{1}{r}\left(2\dfrac{\partial \delta M_r}{\partial r} - \dfrac{\partial \delta M_\theta}{\partial r}\right) + N_r \dfrac{\partial^2 \delta w}{\partial r^2} + \delta N_r \dfrac{\partial^2 w}{\partial r^2} \\ + \delta N_r \dfrac{\partial^2 \delta w}{\partial r^2} + \dfrac{1}{r}\left(N_\theta \dfrac{\partial \delta w}{\partial r} + \delta N_\theta \dfrac{\partial w}{\partial r} + \delta N_\theta \dfrac{\partial \delta w}{\partial r}\right) + \delta q = 0, \end{cases} \tag{8}$$

where w is the mid-plane displacement in the z-direction, q is the external load, $\delta(\cdots)$ stands for a small increment of $(\cdots)$, and

$$(N_r, N_\theta, M_r, M_\theta) = \int_{-h/2}^{h/2} (\sigma_r, \sigma_\theta, z\sigma_r, z\sigma_\theta) \cdot \mathrm{d}z \tag{9}$$

are the membrane forces and the bending moments in the radial and circumferential directions, respectively.

3.1.2. *Geometrical relations.* Von Karman's non-linear relations between strains and displacements are

$$\left.\begin{aligned} \delta\varepsilon_r^0 &= \frac{\partial \delta u}{\partial r} + \frac{\partial w}{\partial r}\frac{\partial \delta w}{\partial r} + \frac{1}{2}\left(\frac{\partial \delta w}{\partial r}\right)^2, \\ \delta\varepsilon_\theta^0 &= \frac{\delta u}{r}, \\ \delta K_r &= -\frac{\partial^2 \delta w}{\partial r^2}, \\ \delta K_\theta &= -\frac{1}{r}\frac{\partial \delta w}{\partial r}, \end{aligned}\right\} \tag{10}$$

where u is the radial mid-plane displacement, ε_r^0 and ε_θ^0 are mid-plane strains in the r- and θ-directions, respectively, and K_r and K_θ are the corresponding curvatures.

3.1.3. *Constitutive equations.* The simple J_2 flow theory, i.e. the Prandtl–Reuss relation, is used. That is (refer to [3], for instance) in the elastic region:

$$\delta\varepsilon_{ij} = \frac{\delta\sigma_{ij}}{2G} - \frac{\nu}{E}\delta\sigma_{kk}\delta_{ij}; \tag{11a}$$

in the plastic region:

$$\delta e_{ij} = \frac{\delta s_{ij}}{2G} + \frac{\partial \phi}{\partial \sigma_{ij}}\delta\lambda, \tag{11b}$$

$$\delta\varepsilon_{kk} = \frac{1-2\nu}{E}\delta\sigma_{kk}, \tag{11c}$$

and

$$\delta\lambda = \begin{cases} 0, & \text{when } \phi(\sigma_{ij} + \delta\sigma_{ij}) \leqslant 0 \\ h^* \delta\phi, & \text{when } \phi(\sigma_{ij} + \delta\sigma_{ij}) > 0, \end{cases} \tag{11d}$$

where v is Poisson's ratio, E is Young's modulus, G is the shear modulus, e_{ij} are the deviatoric strain components, s_{ij} are the deviatoric stress components, ϕ is the Mises loading function and h^* is the work-hardening modulus.

3.2. *Analysis and discussion of examples*

It is easy now to obtain numerical results for the problem named in the title by the maDR method, after the basic equations above are changed into corresponding finite difference ones. The computer program associated with the present paper is composed of two large cycles, see Fig. 2. The inner cycle is the iteration cycle of the maDR method. The iterations are carried out for the pseudo-time. The outer cycle is an external loading one. The algorithm for the maDR method is outlined in the Appendix. It is necessary for an external load to be increased step by step until the total load level is reached.

Both our experimental study and our numerical calculations were carried out for workpieces of thicknesses 1.5 mm and 2 mm, with diameters 120 mm and 150 mm, respectively. The diameters of the cylindrical punches are 45 mm and 65 mm, respectively. The workpieces were made of cold-rolled steel sheet. Its stress–strain curves in the 0, 45 and 90° directions with respect to the rolling direction and their average curve are shown in Fig. 3. The sheet is considered to be an isotropic material, and the average curve is used throughout the calculations. For the sake of convenience, considering that the material hardening curve slopes gently, we simplify the hardening curve to that of a bilinear model—i.e. we take

$$E_t^0 = \begin{cases} 145.0 & \text{when } Y \leqslant \sigma \leqslant 27.5, \\ 62.2 & \text{when } \sigma > 27.5, \end{cases} \quad (\text{kg mm}^{-2}) \tag{12}$$

for the sheet of thickness 2 mm; for that of thickness 1.5 mm,

$$E_t^0 = \begin{cases} 151.1 & \text{when } Y \leqslant \sigma \leqslant 28.1, \\ 53.7 & \text{when } \sigma > 28.1, \end{cases} \quad (\text{kg mm}^{-2}) \tag{13}$$

where E_t^0 is the tangent modulus and Y denotes the initial yield stress.

The following notation is convenient for further discussions:

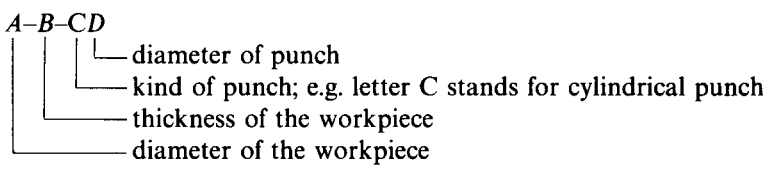

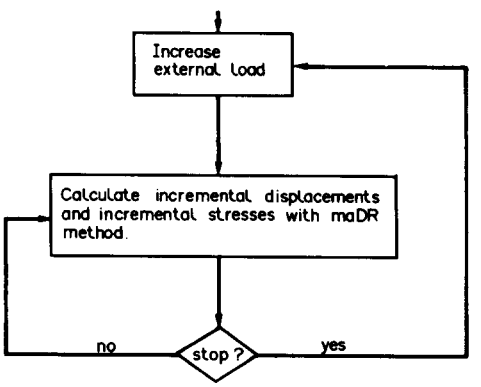

FIG. 2. Flow chart of the computer program.

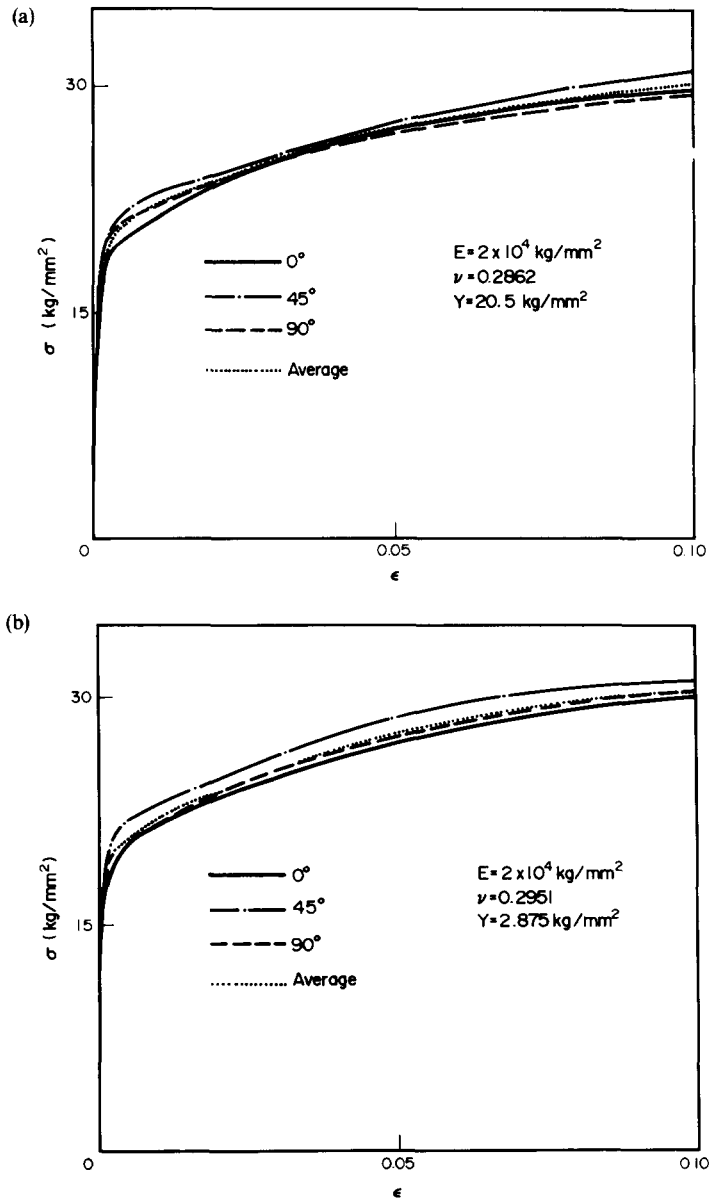

FIG. 3. Stress–strain curves of cold-rolled steel sheets: (a) the sheet of thickness 2 mm; (b) the sheet of thickness 1.5 mm.

For example, 150-2.0-C45 stands for the workpiece of initial diameter 150 mm and thickness 2 mm pressed by a cylindrical punch of diameter 45 mm.

Part of our numerical results are shown in Figs 4–11, and compared carefully with our experimental ones. It can be noted that they are in very good agreement with each other.

Figure 4(a, b) shows the whole processes of loading and unloading of the workpieces 150-2.0-C45 and 120-1.5-C45. They show that the springbacks of the workpieces are slight compared to the case of a plate bent to a shape of single curvature.

Figure 5(a, b) reveals the spread of the plastic regions in the radial sections of workpieces 150-2.0-C45 and 150-2.0-C65. It is found that the plastic regions of two identical workpieces behave differently if subjected to punches with different diameters. For 150-2.0-C45, the upper plastic region first appears at the central part of the sheet, and then spreads to periphery with unloading at the original part inside the circle of the ring load. However, for 150-2.0-C65, the spread and unloading occur before the upper plastic region reaches the

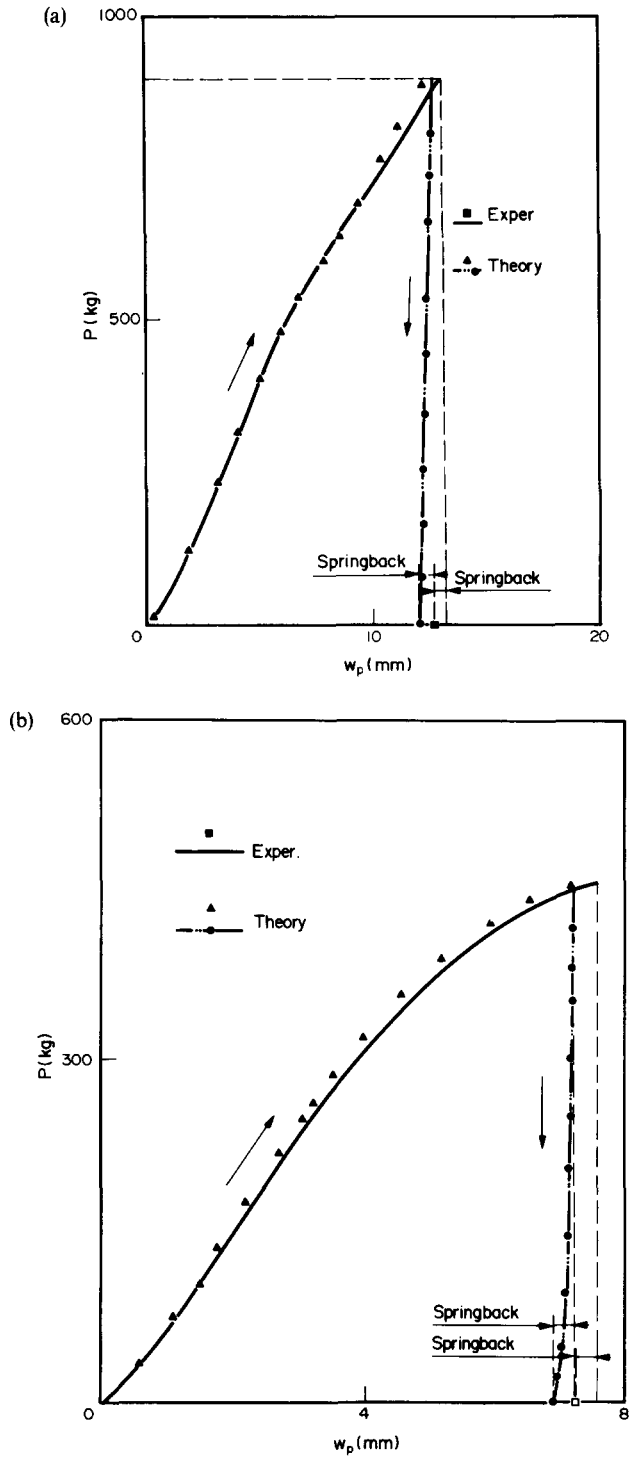

FIG. 4. External load (P)–punch displacement (w_p) curves: (a) 150-2.0-C45; (b) 120-1.5-C45.

central axis. It should be noted that only the sheet elements inside the circle of the ring load undergo a complicated loading and unloading process, while the elements outside the circle are always in a loading state. It follows from this behavior that the validity of Lu and Sayir's method [4] of studying the evolution of plastic regions under the assumption that plastic regions appear first inside the circle of ring load and spread with no unloading is very limited by the diameter of ring load.

The distributions of circumferential membrane forces, N_θ, of 150-2.0-C45 and 150-2.0-C65 and their variations with external load are shown in Fig. 6 parts (a) and (b),

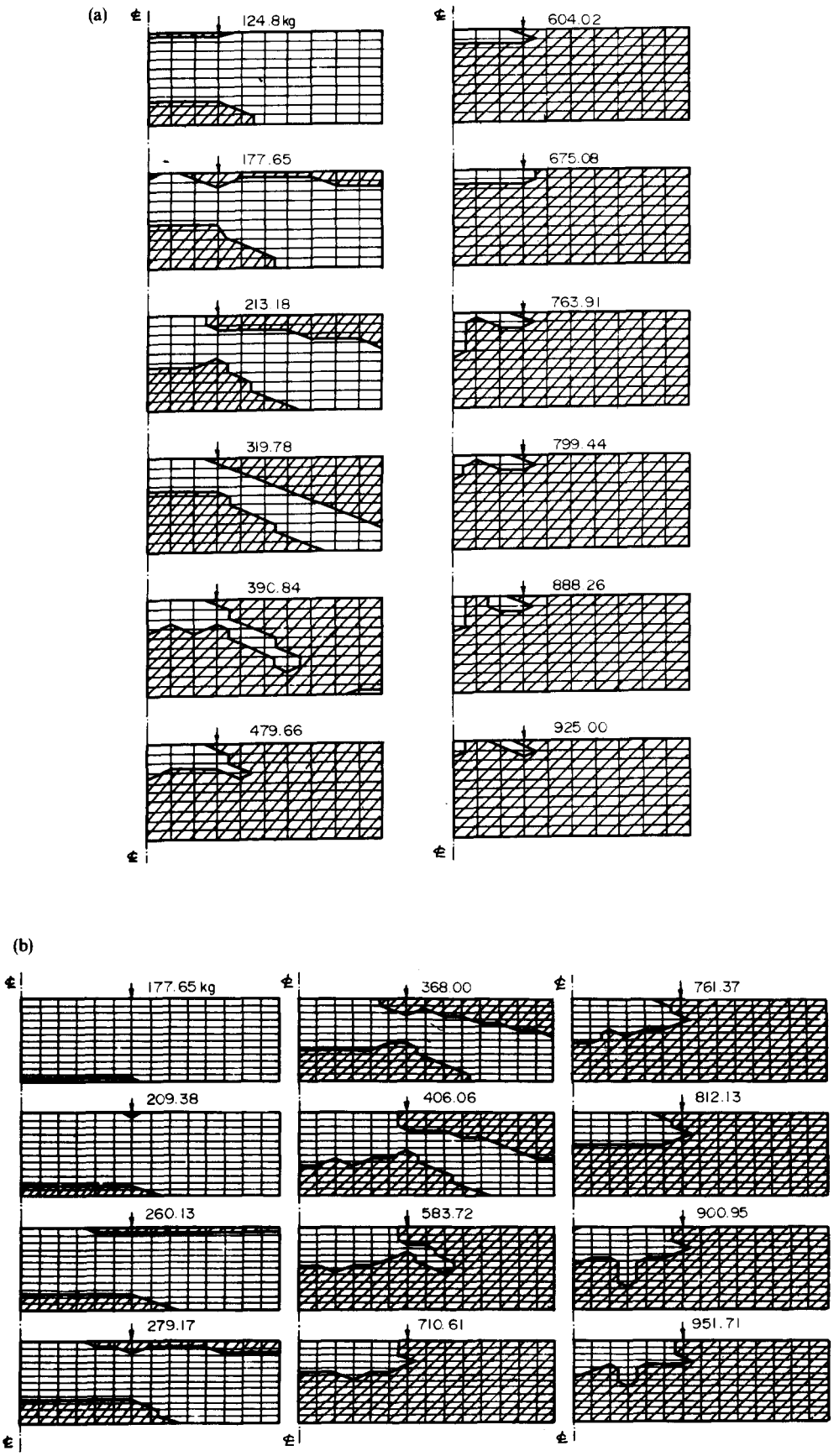

FIG. 5. Evolution of plastic regions with increasing load: (a) 150-2.0-C45; (b) 150-2.0-C65.

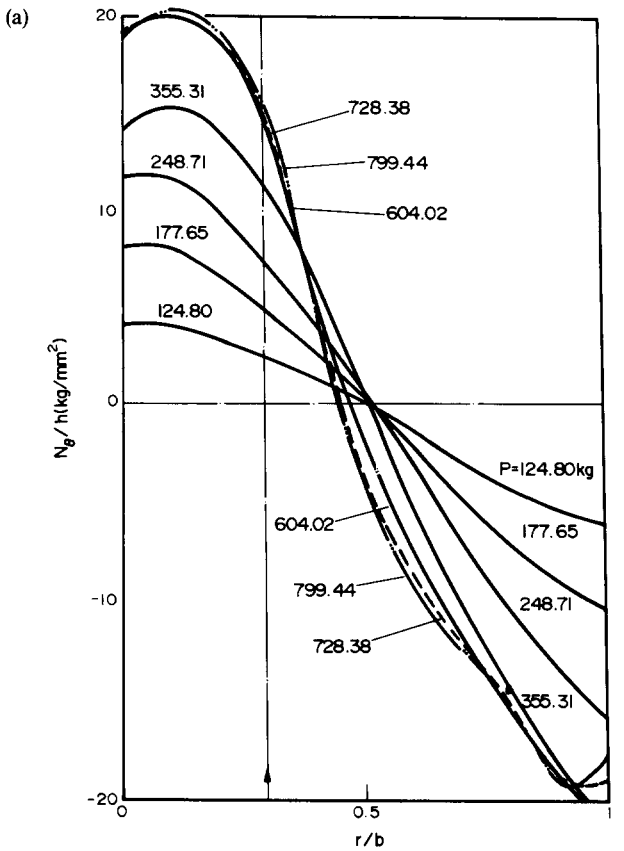

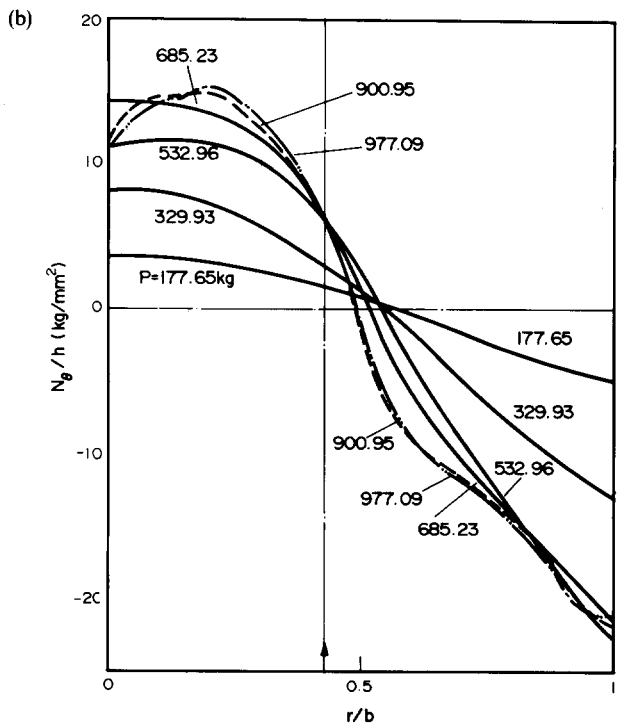

FIG. 6. Distributions of N_θ: (a) 150-2.0-C45; (b) 150-2.0-C65.

respectively. The figure indicates that the variation of N_θ in the neighborhood of the circle of the ring load is sharp, and a band of negative value of N_θ exists outside the load circle. This band is the essential factor which causes circumferential wrinkling. It should be noted that the position of maximum negative value of N_θ moves from the periphery to the interior as the external load increases to a certain value, which makes the curve of N_θ bend near the periphery.

Figure 7 exhibits the curves of the distribution of radial strain ε_r and circumferential strain ε_θ on surfaces $z = \pm h/2$. It confirms that the deformation process can be regarded as one that deforms with large displacements but small strains, because the strains are small except in the very narrow region around the load circle. It is to be expected that the radial strain on $z = h/2$ is positive. However, the fact that positive ε_r appears on part of the surface $z = -h/2$ is unexpected. Nonetheless, if one has noted that a workpiece in the conical cup test is supported on the periphery of $z = h/2$, and hence there exists a negative bending moment applied to the boundary [see Fig. 1(b) and equation (7)], then ε_r near the periphery (on $z = -h/2$) must indeed be positive. (Other small positive values of ε_r are due to computational errors.)

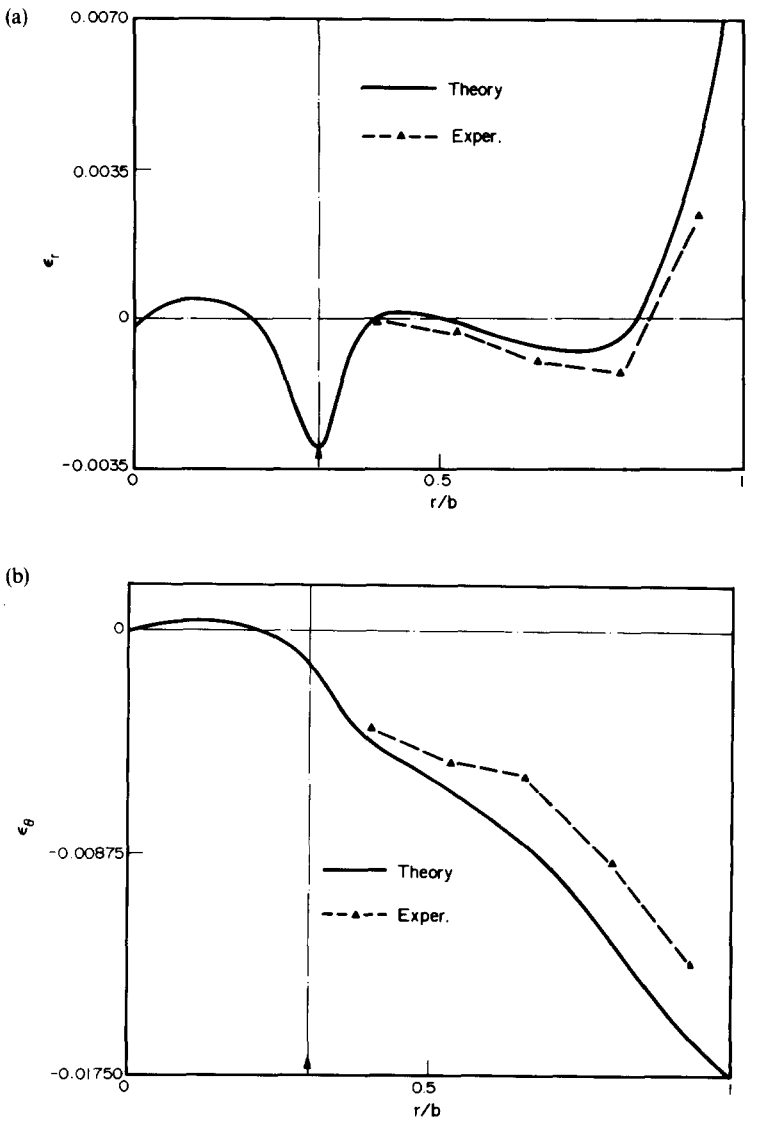

FIG. 7. (a) and (b).

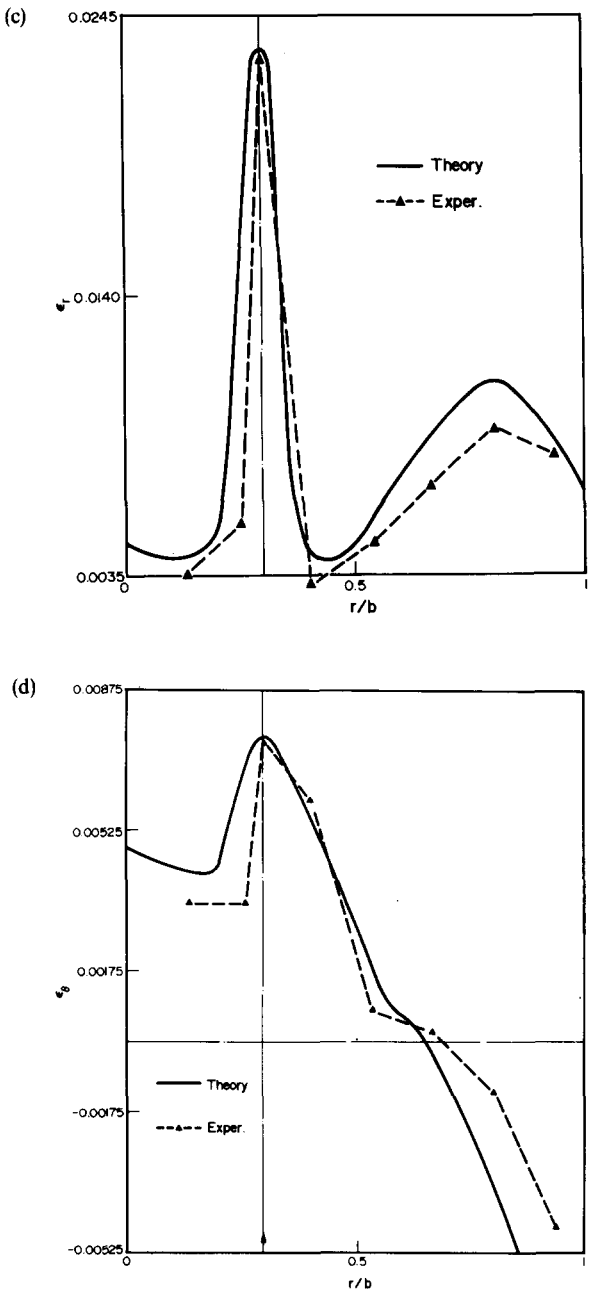

FIG. 7. Distributions of strain components of 150-2.0-C45 (external load $P = 800$ kg): (a) ε_r on $z = -h/2$; (b) ε_θ on $z = -h/2$; (c) ε_r on $z = h/2$; (d) ε_θ on $z = h/2$.

It is easy to imagine that there would be a region of high curvature around the circle of ring load. However, Fig. 8 shows that there exists another high curvature area near the edge of the blank. Moreover, according to systematic numerical analyses, the authors find that the peak of the latter moves slightly to the periphery as the punch advances. It is very much related to the variation of the radial bending moment M_r. It is obvious from Fig. 9 that as the external load increases to a certain extent, a peak in M_r appears at the position corresponding to that of the latter high curvature area.

The radial displacement, u, of the plate elements inside the load circle is very small [see Fig. 10(a)]. Furthermore, the deflection relative to where the load acts and the slope of the

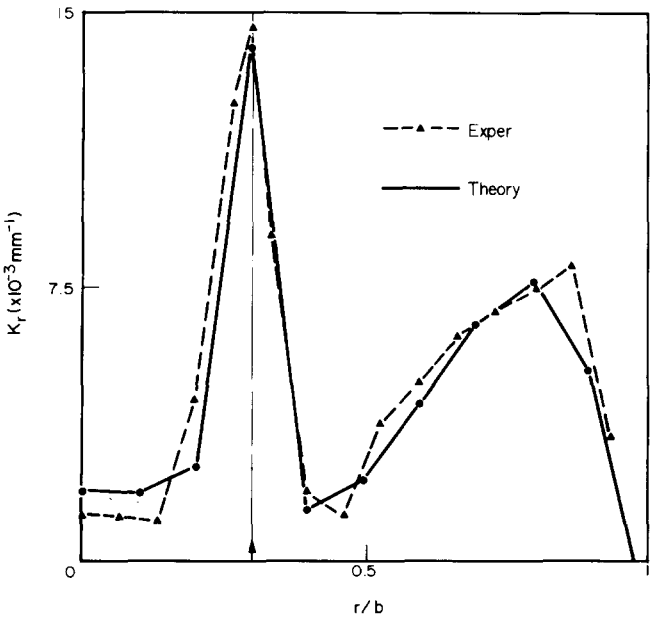

FIG. 8. Distributions of radial curvature of 150-2.0-C45 unloaded at $P = 900$ kg.

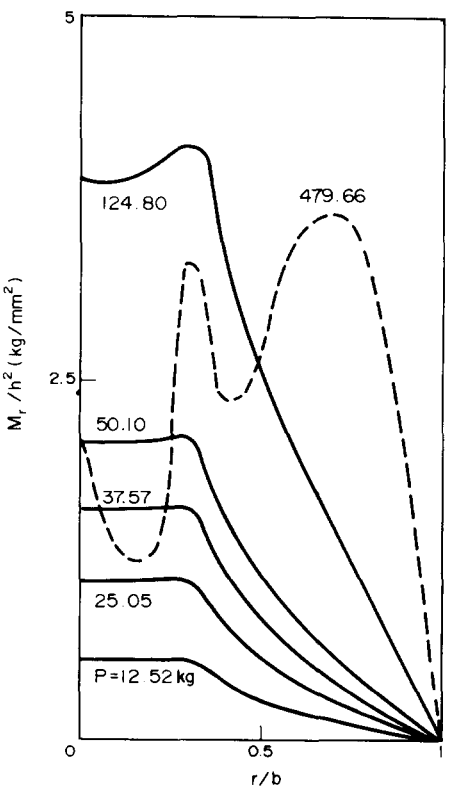

FIG. 9. Distributions of radial bending moment of 150-2.0-C45.

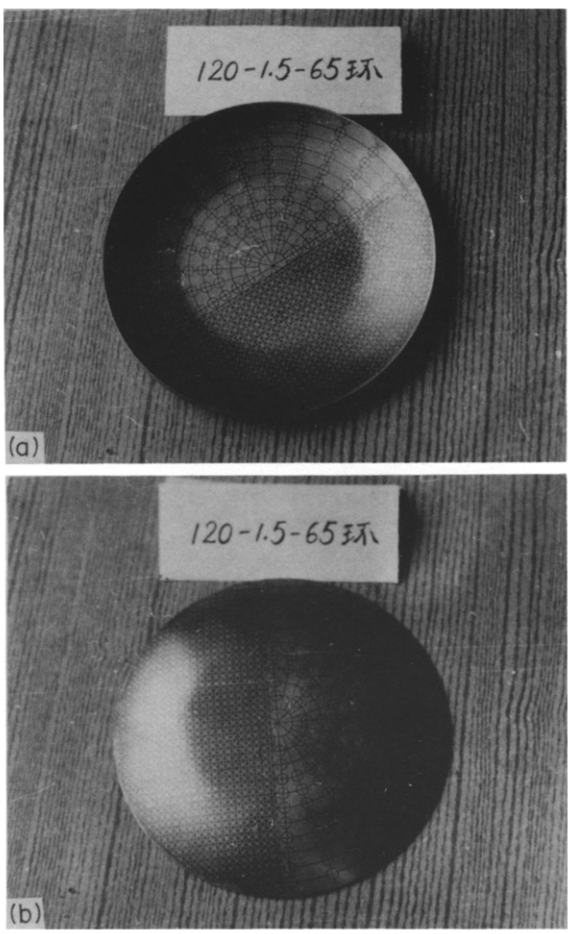

FIG. 11. Photographs of a workpiece after unloading: (a) loaded surface; (b) back surface.

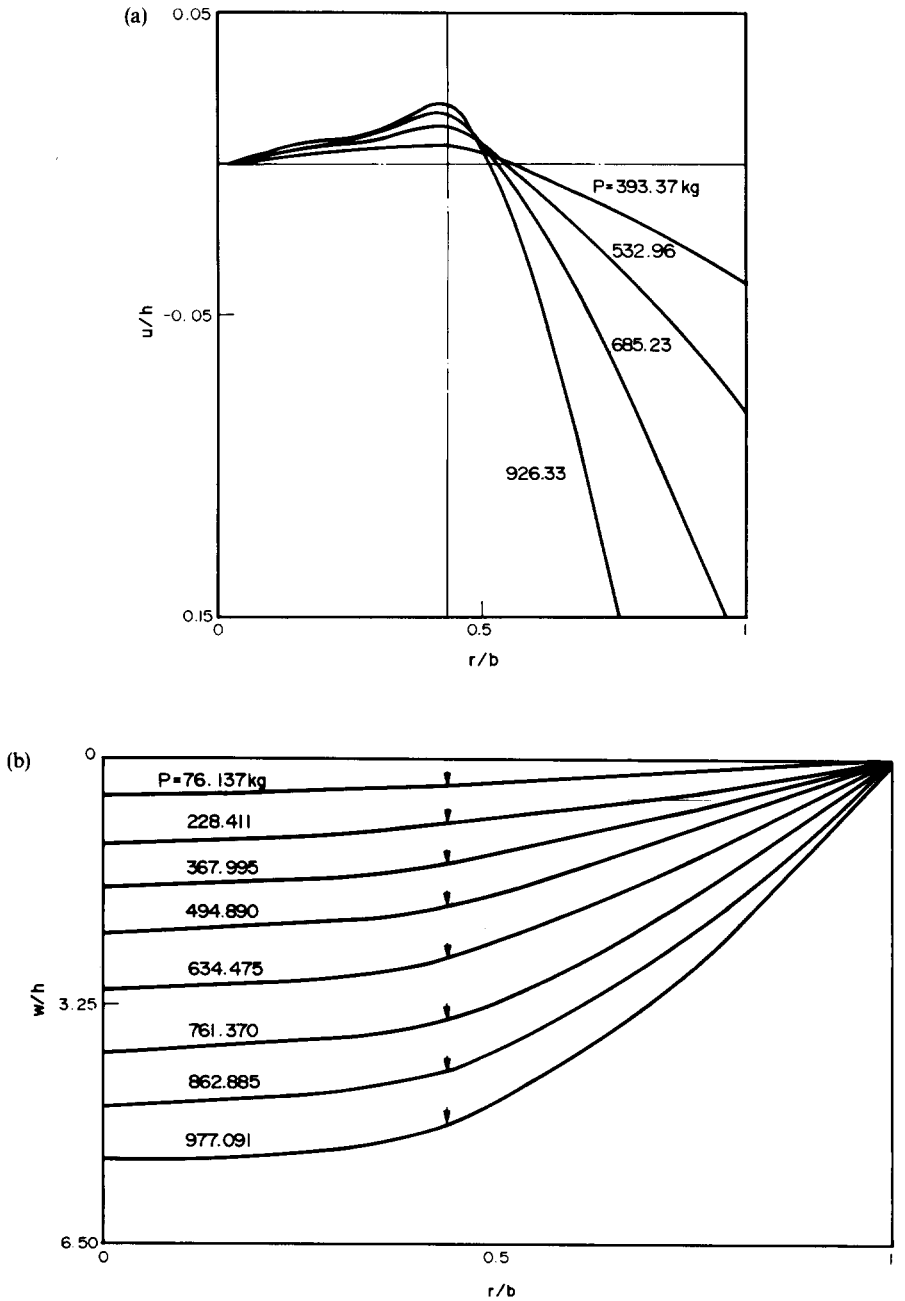

FIG. 10. Distributions of mid-plane displacements of 150-2.0-C65: (a) radial displacement; (b) vertical displacement.

deflection are small [see Fig. 10(b)]. Therefore, an approximate analytical deformation model of such a workpiece for engineers can be obtained on the basis of "the plate elements inside the load circle being considered as rigid and deformations occurring only in those regions outside the circle". The photographs in Fig. 11 provide objective pictures for the model.

4. CONCLUSIONS

It follows from the above analyses and discussions that:

(1) the maDR method is very efficient for solving the highly non-linear problems of sheet metal forming;

(2) the evolution of the plastic regions in a workpiece is closely related to the variation of punch diameter;
(3) the movement of the position of maximum negative value of N_θ may affect the plastic wrinkling of the workpiece;
(4) the deformation process of a workpiece can be considered as one that undergoes large displacements with small strains;
(5) the approximate analytical model proposed here may prove useful for production engineers.

Acknowledgements—The authors would like to acknowledge the support of the Chinese National Natural Science Foundation for this research. They also wish to express their thanks to Professor W. Johnson for helpful comments on an earlier draft of this work.

REFERENCES

1. L. C. ZHANG, T. X. YU and R. WANG, The maDR method and its applications (to be published).
2. P. UNDERWOOD, Dynamic relaxation. In *Computational Methods for Transient Analysis*, Chap. 5. (Edited by T. BELYTSCHKO and T. J. R. HUGHES). Elsevier, New York (1983).
3. R. HILL, *The Mathematical Theory of Plasticity*. Oxford University Press (1950).
4. M. W. LU and M. SAYIR, An analytical asymptotic approximation to the deformation of an elastic–plastic plates. *ZAMP* **33**, 443–460 (1982).

APPENDIX

The algorithm of maDR method can be expressed as

(1) compute $\mathbf{M}$; $\mathbf{X}^0 = \dot{\mathbf{X}}^0 = \mathbf{0}$; $c^0 = 0$,
(2) calculate $\bar{\mathbf{X}} = (\mathbf{X}^* + \mathbf{X}^{**})/2$,
(3) $\mathbf{X}^0 = \bar{\mathbf{X}}$ and $\dot{\mathbf{X}}^0 = \mathbf{0}$,
(4) e_{KE}, e_{RR}, and N given; $n = 0$,
(5) compute $\mathbf{M}$ again,
(6) calculate $\mathbf{R}^n$,
(7) if $|R_i^n| \leqslant e_{RR}$ stop, otherwise continue,
(8) calculate $\dot{\mathbf{X}}^{n+1/2}$ and $c^n(\dot{\mathbf{X}}^{1/2} = \tau^0 \mathbf{M}^{-1}\mathbf{R}^0/2)$,
(9) if $\sum_j (\dot{x}_j^{n+1/2})^2 \leqslant e_{KE}$ stop; otherwise continue,
(10) determine $\mathbf{X}^{n+1}$,
(11) exert boundary conditions,
(12) $n = n + 1$,
(13) if $n \geqslant N$ stop; otherwise return to step (5).

Throughout the present calculations, values of $e_{KE} = 1.\,E-10$, $1.E-15$ and $e_{RR} = 1.E-6$ were assumed. The values of N in different examples were different.